

Spectral characteristics of ultrashort pulses in Kerr-lens mode-locked lasers

V.L. Kalashnikov, E. Sorokin, and I.T. Sorokina

Institut für Photonik, TU Wien, Gusshausstr. 27/387, A-1040 Vienna, Austria

ABSTRACT

A number of factors that influence spectral position of the femtosecond pulse in a Kerr-lens modelocked Cr:LiSGaF laser have been identified: high-order dispersion, gain saturation, reabsorption from the ground state, and stimulated Raman scattering. Using the one-dimensional numerical model for the simulation of the laser cavity, the relative contributions of different factors have been compared. The Raman effect provides the largest self-frequency shift from the gain peak (up to 60 nm), followed by the gain saturation (~ 25 nm), while the high-order dispersion contribution is insignificant (~ 5 nm). Comparison with the experimental data confirm that the stimulated Raman scattering is a main cause of the ultrashort pulse self-frequency shift observed in Cr:LiSGaF and Cr:LiSAF lasers.

Keywords: ultrashort pulses, Kerr-lens mode-locking, stimulated Raman scattering

1. INTRODUCTION

A rapid progress in Kerr-lens mode-locking technique allows to reach 14 and 12-fs pulse durations in Cr:LiSGaF and Cr:LiSAF lasers, respectively.^{1,2} These active media are attractive due to possibilities of sub-20 fs pulse generation directly from the diode-pumped laser. At the same time, the lasers demonstrate a significant Stokes shift of the pulse spectrum at such short pulsewidths.^{3,4,1} This shift decreases the accessible bandwidth due to the worse overlap of the gain and the pulse spectra, thus setting a limit to pulse duration.⁴ Therefore, investigation of the nature of the ultrashort pulse spectrum transformation has not only academic but also practical significance.

A number of explanations for the ultrashort pulse spectrum shift in mode-locked lasers have been suggested. For example, it was supposed, that due to the high-order dispersions the spectral region of negative group-delay dispersion, which is optimal for pulse formation, may be displaced.⁵ However in the framework of the perturbation theory the third-order dispersion does not contribute to the pulse carrier frequency, but results in spectrum asymmetry and fragmentation.⁶ Only in the case of the non-steady-state operation there is a possibility for the strong dynamic frequency shift.⁷

A more realistic explanation of the frequency shift takes into account frequency filtering due to reabsorption in the gain medium.² However, as it will be shown below, this explanation can not explain the dependence of the frequency shift on the pulse energy. Moreover, such dependence suggests that a nonlinear mechanism is involved in the frequency shift.

As it was shown in Ref.,⁸ the stimulated Raman scattering in active medium is a very suitable nonlinear process, which can produce the experimentally observed Stokes frequency shift in sub-50 fs domain. The analysis in Ref.⁸ was based on the soliton perturbation theory that did not allow to take into account the effect of high-order dispersion and frequency-dependent dissipative lasing factors such as asymmetric gain band, spectral filtering on the output mirror, reabsorption in the gain medium and gain saturation.

In this work we performed a numerical analysis of the spectral characteristics of ultrashort pulses on the basis of a relatively simple model of the Kerr-lens mode locking (KLM). The main advantages of our model is taking into consideration of the high-order dispersion, exact profiles of the loss and gain bands, frequency dependent reabsorption in the active medium, gain saturation and fast absorber action of the Kerr-lensing. The obtained results are in a good agreement with experimental data and allow to estimate the contribution of the different factors to spectral characteristics of ultrashort pulses.

Further author information: (Send correspondence to Dr. E. Sorokin)

E. Sorokin: E-mail: e.sorokin@tuwien.ac.at

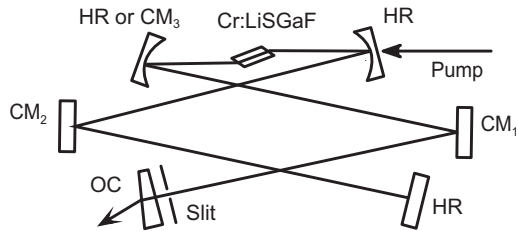


Figure 1. General scheme of a KLM Cr:LiSGaF laser used in this paper. This scheme directly corresponds to the experiments in Refs.^{1,3} HR, high reflector. CM, chirped mirror. OC, output coupler.

The paper is organized as follows: first a summary of relevant measurements and experimental results is given, followed by the construction of the analytical and computational models. We then present the results of our calculations and discuss the influence of each of the abovementioned factors separately. Finally, we present the results of simulation with all factors included, using distributed and discrete-element models.

2. EXPERIMENTAL OBSERVATIONS

Systematic Stokes shift of the ultrashort modelocked pulse in Cr:LiSGaF- and Cr:LiSAF-based KLM oscillators has been first reported in 1997,^{1,3,9} where the stimulated Raman scattering has been suggested as a possible mechanism. It has been found, that i) the shift could be observed in oscillators with different dispersion characteristics, ii) the shift increases with the pulse energy, and iii) the shift increases with pulse shortening. At pulse durations below 20 fs, the peak of the pulse spectrum may shift as far as 50-70 nm into the infrared as compared to the cw wavelength or modelocked spectrum at long pulse durations (~ 840 nm in Cr:LiSGaF).¹ Later, analogous shifts in Cr:LiSAF have been reported by Uemura and Torizuka² and R. Gäbel *et al.*¹⁰ All mentioned experiments used the common optical scheme, differing only in pump arrangements and dispersion compensation techniques. The schematic diagram of the laser oscillator is shown in Fig. 1. This is a representative scheme for any X-shaped KLM laser, because different types of dispersion compensation can always be represented by lumped dispersion of a chirped mirror. For modeling purposes we used the parameters of experiments, reported in Refs.^{1,9}: the Brewster-angled 4 mm long LiSGaF crystal doped with 1.4% Cr, beam diameter in Cr:LiSGaF crystal $40 \times 60 \mu\text{m}$. The high reflectors (HR) had negligible dispersion. The dispersion of the chirped mirrors (CM) has been calculated from its original design, and additionally measured by white-light interferometry. The intracavity dispersion was calculated using the dispersion data of Cr:LiSGaF,³ measured dispersion curves of the chirped mirrors and calculated dispersion of the output coupler (Fig. 2). We also used the experimental loss spectra (mirror transmission and ground-state absorption in Cr:LiSGaF) as shown in Fig. 3.

The laser was pumped by 1.2-1.5 W from a Kr⁺-ion laser at 647 nm, with a TEM₀₀ beam, of which 0.9-1.1 W have been absorbed in the active medium, generating 60-100 mW of average output power in the modelocked regime. The resonator was slightly asymmetric, with distances between the curved mirrors (radii of curvature 100 mm) and end mirrors being 88 and 109 cm, corresponding to 72 MHz pulse repetition rate. Modelocking has been achieved primarily by the hard aperture in form of an adjustable slit close to the output coupler (Fig. 1). Fig. 4 shows normalized output spectra at different pulse peak power, demonstrating the spectral shift. Similar spectral behaviour has been observed also in Cr:LiSAF oscillators. However, for the sake of simplicity we provide experimental data and perform simulations on Cr:LiSGaF only.

The Raman gain spectrum of undoped LiSGaF crystal has been measured according to the procedure described in Ref.,⁹ using the orientated crystalline quartz as a reference, and taking into account the thermal phonon population factor. The spectrum (see Fig. 5) is obtained from spontaneous Raman scattering spectrum, recorded in confocal back-scattering geometry. Both incident and scattered light is polarized along the *c* axis, corresponding to the polarization of light in the laser. LiSGaF possesses spatial symmetry group D_{3d}^2 (P $\bar{3}1c$) with 2 formula units in a unit cell, resulting in total of 32 optical phonon modes $3A_{1g} + 4A_{2g} + 4A_{1u} + 5A_{2u} + 8E_g + 8E_u$, of which $3A_{1g} + 8E_g$ are Raman-active. In the scattering geometry as described above, only 3 full-symmetric A_{1g} modes are visible (Fig. 5), with relevant parameters given in Table 1.

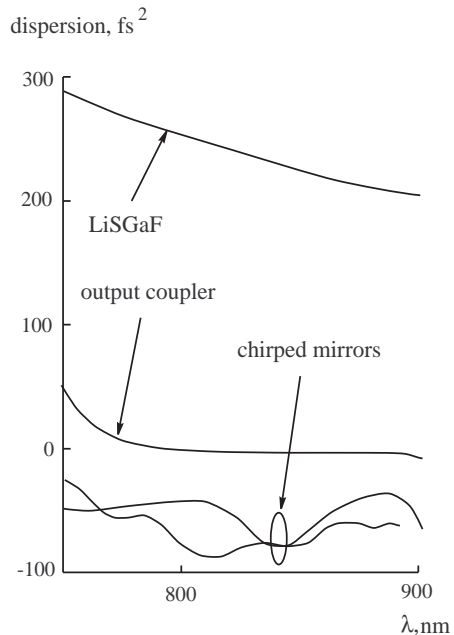


Figure 2. Measured group delay dispersion of the active media (8 mm in double pass), output coupler and chirped mirrors in dependence on the wavelength λ .

Table 1. Raman gain of undoped LiSGaF.

Frequency $\Omega_j/2\pi$ cm^{-1}	Raman gain g_j^s cm/GW	Width (FWHM) cm^{-1}	T_j ps
230	0.014 ± 0.005	9 ± 3	1.2 ± 0.4
349	0.021 ± 0.006	14 ± 2	0.7 ± 0.1
551	0.32 ± 0.05	12.5 ± 0.6	0.86 ± 0.05

3. MODEL

There exist different approaches to modeling of ultrashort pulse generation in solid-state laser, which are based on soliton or fluctuation models. The soliton approach can be applied only the distributed laser model (where the dispersion and nonlinearity are implied to be evenly distributed over the round-trip and act simultaneously) but allows to build comparatively simple analytical description thus promoting easy interpretation of results. We also based our calculations on the distributed laser model but the results were tested by simulations on the basis of discrete-element scheme corresponding to Fig. 1. To overcome the limitations of the soliton approach we used numerical simulations allowing to account for the high-order dispersion, the laser field reabsorption, the complicated spectral profiles of the gain and output coupler transmission, and the Raman scattering within the active medium.

The modelocking is described by a fast absorber-like action of Kerr-lensing in the active medium in the form of a nonlinear transmission-operator $\exp\left[-\frac{\gamma}{1+\sigma|a(z,t)|^2}\right]$,¹¹ where γ is the modulation depth (KLM loss), which is set by the cavity arrangement, σ is the inverse loss saturation intensity, a is the field depending on local time t and longitudinal coordinate z ($|a|^2$ has the meaning of the field intensity). Parameters γ and σ are controlled by changing

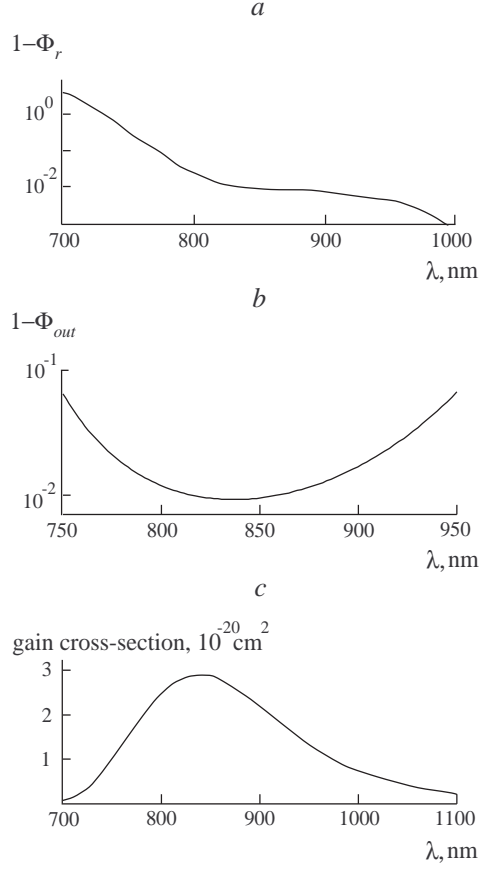


Figure 3. Ground-state absorption of Cr:LiSGaF (a), round-trip resonator losses due to the output coupler (b) and gain cross-section of Cr:LiSGaF (c).

the cavity configuration, which is a common procedure for Kerr-lens mode-locking experiment.

Another fundamental factor in our model is the presence of high-order dispersions due to the active medium, the dispersion compensator, the output coupler, and high-reflective mirrors. The corresponding experimental characteristics are shown in Fig. 2. For the numerical calculations, the data were represented by the eighth-order polynomial approximation. The action of dispersion can thus be presented in the following form:

$$a(z, t) = \int_{-\infty}^{\infty} a(z, t') G(t - t') dt', \quad (1)$$

$$G(t - t') = \frac{1}{2\pi} \int_{-\infty}^{\infty} \exp \left(-i \sum_{j=2}^8 \frac{1}{j!} D_j (\omega - \omega_0)^j - (t - t') \omega \right) d\omega, \quad (2)$$

where ω is the frequency, $G(t - t')$ is the Green's function depending on the dispersion coefficients D_j up to eighth order of j .

The next important factor in our model is the gain saturation that was described on the basis of quasi-two level scheme of the active medium operation ¹²:

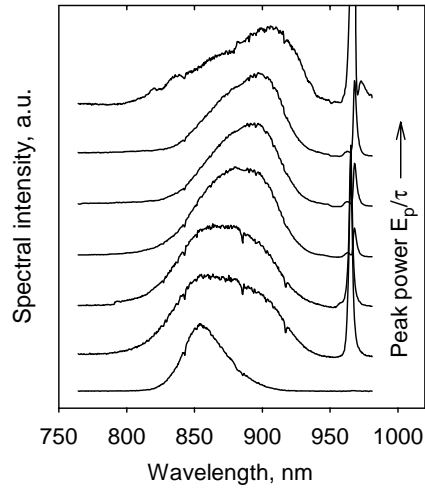


Figure 4. Experimental demonstration of the pulse frequency shift. The output spectra of modelocked Cr:LiSGaF laser, with changing intracavity pulse peak power (bottom spectrum corresponds to the lowest peak power, top spectrum - to the highest peak power).

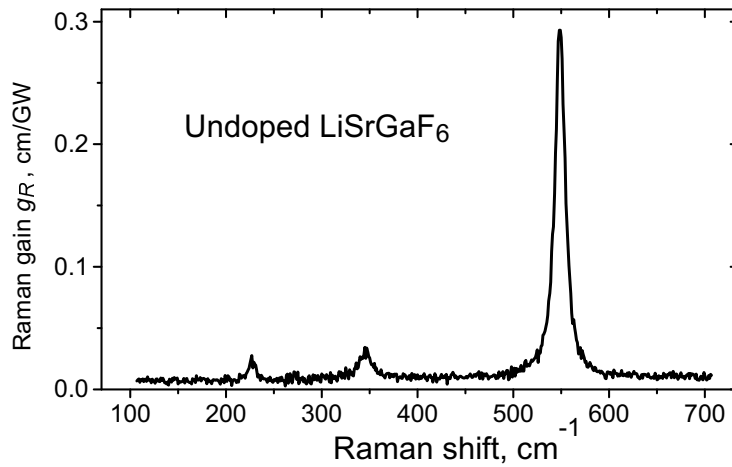


Figure 5. Raman gain of undoped LiSGaF. Exciting laser line at 514.5 nm and scattered light are both polarized along the crystallographic z axis, corresponding to the polarization of the laser radiation in Cr:LiSGaF laser.

$$\frac{\partial \alpha}{\partial t} = \frac{I_p \sigma_{14}}{h\nu} (\alpha_{\max} - \alpha) - \frac{|a|^2 \sigma_{32}}{h\nu} \alpha - \frac{\alpha}{T_r} \quad (3)$$

where I_p is the pump intensity, ν is the pump frequency, σ_{14} and σ_{32} are the loss and the gain cross-sections, respectively, $T_r = 85 \mu\text{s}$ is the gain relaxation time. If the pulse duration is much less than cavity round-trip time $T_{cav} = 14 \text{ ns}$, then this equation can be replaced by the following one:

$$\frac{\partial \alpha}{\partial z} = P (\alpha_{\max} - \alpha) - \frac{E}{E_s} \alpha - \frac{T_{cav}}{T_r} \alpha \quad (4)$$

where $P = (I_p \sigma_{14} / h\nu) T_{cav}$ is the dimensionless pump intensity, z is the dimensionless longitudinal coordinate, i. e. the number of the cavity round-trips. $E_s = h\nu / \sigma_{32}$ is the gain saturation energy flux, E is the full pulse energy flux.

Self-phase modulation in the active medium was represented by nonlinear ‘‘transmission’’ operator $\exp[-i\beta |a(z, t)|^2]$, where $\beta = 2\pi n_2 x / \lambda n = 3.4 \text{ cm}^2 / \text{TW}$ is the self-phase modulation coefficient. Here n and n_2 are the linear and non-linear coefficients of refraction, respectively, λ is the central wavelength corresponding in our case to the gain band maximum, $x = 8 \text{ mm}$ is twice the length of the active crystal.

Finally, we consider the stimulated Raman scattering within the active medium. Following Ref. ,⁸ where Raman scattering contribution was calculated analytically on the basis of the soliton model, we supplement the model with the following equations:

$$\frac{\partial a_s}{\partial \varsigma} = i \sum_{j=1}^3 Q_j^* a_p, \quad (5)$$

$$\frac{\partial a_p}{\partial \varsigma} = i \sum_{j=1}^3 Q_j a_s, \quad (6)$$

$$\frac{\partial^2 Q_j}{\partial t^2} + \frac{2}{T_j} \frac{\partial Q_j}{\partial t} + \Omega_j^2 Q_j = \mu_j a_p a_s^*, \quad (7)$$

where ς is the longitudinal coordinate (pulse propagation axis) inside the active medium, $a_{p,s}$ are the amplitudes of the ‘‘pump’’ and the ‘‘Stokes’’ components within generation spectrum, Ω_j are the phonon resonance frequencies ($j = 1, 2, 3$ corresponding to the three Raman-active phonon resonances in LiSGaF, see Fig. 5). T_j are the inverse bandwidths of Raman lines, $\mu_j = g_j^s \Omega_j / T_j$ are the coupling parameters for Raman gain coefficients g_j^s .

Solving third equation of the system, we obtain the steady-state phonon amplitude for the fixed pump and the Stokes components with corresponding frequencies ω_p and ω_s :

$$Q_j = \frac{\mu_j a_p a_s^*}{\Omega_j^2 - \frac{2i(\omega_p - \omega_s)}{T_j} - (\omega_p - \omega_s)^2} \approx \frac{\mu_j a_p a_s^*}{2\Omega_j (\Omega_j - (\omega_p - \omega_s)) - \frac{2i\Omega_j}{T_j}}. \quad (8)$$

The validity of the last approximate expression follows from the fact that the Raman lines are narrow in comparison with the pulse spectrum. With regard to the contribution of all spectral components of the pulse to the phonon amplitude, the equation for the Stokes and the pump fields in the frequency domain can be written as:

$$\frac{\partial a_s}{\partial \varsigma} = i a_s \sum_{j=1}^3 \mu_j \sum_k \frac{|a_{p,k}|^2}{2\Omega_j (\Omega_j - (\omega_{p,k} - \omega_s)) + \frac{2i\Omega_j}{T_j}} \quad (9)$$

$$\frac{\partial a_p}{\partial \varsigma} = i a_p \sum_{j=1}^3 \mu_j \sum_k \frac{|a_{s,k}|^2}{2\Omega_j (\Omega_j - (\omega_p - \omega_{s,k})) - \frac{2i\Omega_j}{T_j}} \quad (10)$$

where k is the index of the field's spectral (i.e. Fourier) component (in the simulations we considered 2^{13} components). Since the Raman lines are narrow, the field variation within these lines is negligible, i.e. $a_{s,p}$ are constant and can be taken out of the second summation. Then the summation can be executed explicitly by transition to the integral, resulting in

$$\frac{\partial a_s}{\partial \varsigma} = \frac{\pi}{4} \sum_{j=1}^3 a_s g_j^s |a_p|^2, \quad (11)$$

$$\frac{\partial a_p}{\partial \varsigma} = -\frac{\pi}{4} \sum_{j=1}^3 a_p g_j^s |a_s|^2. \quad (12)$$

It should be noted, that in these equations $\omega_p - \omega_s = \Omega_j$ and there is the pair-wise interaction of the spectral components within the wide enough generation spectrum.

There are two main mechanisms of the generation of the initial seed at the Stokes frequency for Eqs. (3). The first one is the spontaneous Raman scattering with the increments of the scattered intensity growth

$$\chi_j = \frac{\omega_p \omega_s^2 n_s^2 \hbar g_j^s}{\pi c^2 \left[1 - \exp\left(-\frac{\hbar \Omega_j}{k_B T}\right) \right]}, \quad (13)$$

where n_s is the index of refraction at Stokes frequency, T is the temperature, and k_B is the Boltzmann's constant.¹³ With this seed signal, the stimulated Raman scattering results in appearance and growth of spectral replicas of the main oscillation pulse, shifted to the lower frequencies by the Raman frequencies Ω_j .

More significant source for Stokes component's amplification, however, is the broad-band pulse field itself. When the pulse spectrum is wide enough to become comparable with the Raman frequency shift, the lower-frequency part of the spectrum can play a role of the Stokes component seed with respect to the higher-frequency part of the spectrum. The stimulated Raman scattering then transfers the energy from the higher-frequency components to the lower-frequency ones, resulting in the continuous red-shift of the pulse spectrum as a whole. As the field amplitude of the laser pulse significantly exceeds the spontaneous seed, the second mechanism strongly dominates over the first one. However, we included both mechanisms in our model, because their influence on the pulse spectrum is quite different.

Later on it is convenient to normalize the time to the inverse gain bandwidth $t_g = 2.25$ fs and the intensity to β^{-1} , resulting in the normalization of the field energy to $(\beta t_g)^{-1}$. As already pointed out, we analyzed the described above model in two ways: on the basis of distributed and discrete-element approaches. In the framework of the distributed model, we didn't consider the propagation through the individual laser element and supposed that the pulse envelope is formed by the overall net-dispersion in the cavity. As result we have a split-step scheme describing ultrashort pulse propagation from z to $z + 1$ transits:

$$a(z', t) = \int_{-\infty}^{\infty} \dots \int_{-\infty}^{\infty} a(z, t') C(t - t') L(t' - t'') A(t'' - t''') G(t''' - t'''') dt' dt'' dt''' dt'''' , \quad (14)$$

$$a(z + 1, t) = a(z', t) \exp\left(-\frac{\gamma}{1 + \sigma |a(z', t)|^2} - i |a(z', t)|^2\right), \quad (15)$$

$$\alpha(z + 1) = \alpha(z) \exp\left(-\tau \int_{-\infty}^{\infty} |a(z, t')|^2 dt' - T_{cav}/T_r - P\right) + \frac{P \alpha_{\max} (1 - \exp(-T_{cav}/T_r - P))}{P + T_{cav}/T_r}, \quad (16)$$

where $\tau = t_g/(E_s\beta) = 0.00079$ is the normalized gain saturation parameter. The Green's functions A , L , C describe spectral bands of gain, reabsorption and output loss, respectively (note, that the dispersion is already included in G):

$$A(t-t') = \frac{1}{2\pi} \int_{-\infty}^{\infty} (1 + \alpha(z)) \Phi_{\alpha}(\omega) \exp[i\omega(t-t')] d\omega, \quad (17)$$

$$L(t-t') = \frac{1}{2\pi} \int_{-\infty}^{\infty} \Phi_r(\omega) \exp[i\omega(t-t')] d\omega, \quad (18)$$

$$C(t-t') = \frac{1}{2\pi} \int_{-\infty}^{\infty} \Phi_{out}(\omega) \exp[i\omega(t-t')] d\omega, \quad (19)$$

Here, $\Phi_{\alpha, r, out}$ are the “form-factors” describing spectral profiles of the gain, reabsorption and the output coupler bands, which resulted from the functional approximation of the experimental data (Fig. 3).

The system (3) has to be completed by the system (3) and the result can be solved on the basis of numerical simulation in Fourier domain and split-step method for nonlinear propagation.

The discrete-element approach is based on the element-to-element simulation of the pulse propagation through the cavity on every round-trip, following the laser scheme in Fig. 1. The nonlinear and spectral characteristics of each laser element are considered separately. Further refinement of the simulation is achieved by considering the pulse propagation through active medium by splitting it into five slices and applying the split-step procedure to each slice consecutively.

4. DISCUSSION

Our simulations are aimed at investigation of the influence of the different factors on spectral characteristics of the ultrashort pulses. Therefore, to simplify the interpretation, we will first consider the high-order dispersion action without Raman scattering and without reabsorption; then reabsorption and Raman scattering will be taken into consideration without high-order dispersion action; and finally, the join action of all factors will be analyzed. To conclude, we will also compare the obtained results with the calculation based on the discrete-element model.

4.1. High-order dispersion action

As it was discussed in,⁶ small contribution of third-order dispersion to characteristics of Schrödinger soliton does not cause the frequency shift, but introduces additional field time delay on the cavity round-trip. However, the influence of the linear and nonlinear dissipative terms in Eqs. (3) can destroy the soliton character of the pulse, in particular, it can add the chirp. The latter, as it was shown in,⁷ results in the frequency shift of the pulse spectrum in the non-steady-state regime. Additionally, in the real-world laser systems the contribution of the high-order dispersions, as a rule, lies beyond the bounds of the perturbation theory validity.

The typical net-dispersion curves corresponding to the experiment with the chirped mirrors are presented in Fig. 6, *a*. Over the full spectral region of generation the pulse undergoes the non-negligible influence of the dispersion up to the eighth-order (see Eq. (2)). As a rule, there is the closed spectral window of dispersion, which is “optimal” for steady-state pulse generation. The contribution of the high-order dispersion terms can shift this window. In Fig. 6, *a*, this shift corresponds to the red-shift of the positive net-dispersion branches (transition from solid to dash and dot curves). The resulting output spectra obtained from the distributed model are shown in Fig. 6, *b*. The net-dispersion shift is accompanied by the red-shift of the pulse spectrum (transition from solid to dash and dot curves). Besides this effect there is the possibility of the essential spectral profile distortion (solid curve) and side-band generation (side-bands lie outside the of shown region).⁴

However, we cannot consider this shift as the cause of the experimentally observed effect because the dispersion shift has the linear nature, i. e. there is no obvious dependence of this shift on the field energy. This is demonstrated

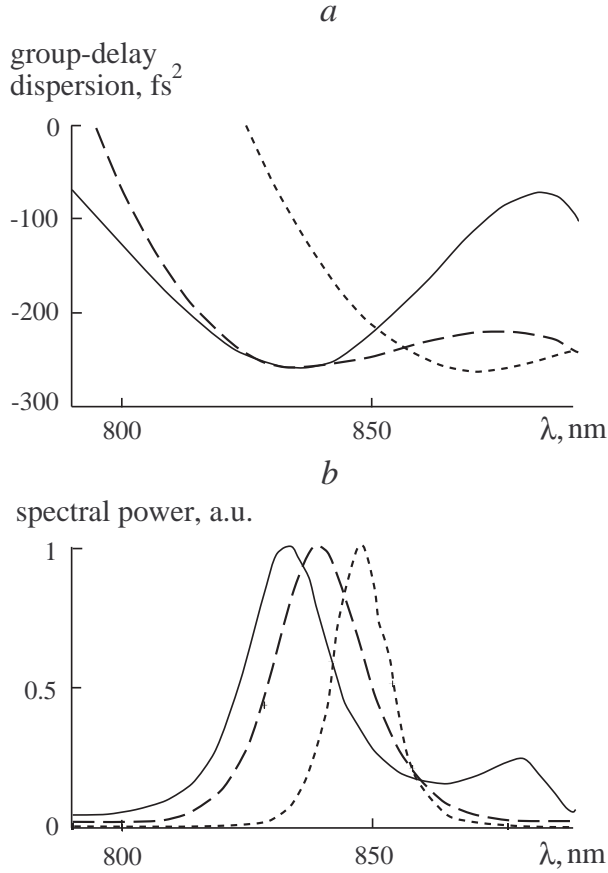


Figure 6. The dependence of dispersion (a) and generation spectra (b) on wavelength. $P = 3.2 \times 10^{-4}$, $\sigma = 1$, $\gamma = 0.05$, pulse energy E is 20 nJ. Pulse durations t_p : 27 (solid curve), 38 (dash), 36 fs (dot).

by Fig. 7, where the pulse energy variation due to the pump variation changes the spectral profile, but does not cause any noticeable frequency shift (compare solid and dash curves in this figure).

The obtained results demonstrate that the self-frequency shift cannot be caused by the non-dissipative factors. As the pulse duration is too large for the nonlinear dispersion to play any significant role, we will concentrate on spectrally-dependent losses and Raman effect.

4.2. Output loss and reabsorption in gain medium

As mentioned above, dependence of the frequency shift on pulse energy implies the involvement of some nonlinear mechanism. Since in the real-world systems the gain band does not coincide with filtering band (output mirror in our case) and the reabsorption band, the spectral position of the net-gain maximum changes with the gain value. The latter is defined by the pump and by the pulse energy (see Eqs. (3)): pulses with higher energy experience lower gain due to the multi-pass saturation. The dependence of the net-gain maximum on the saturated steady-state gain coefficient α is shown in Fig. 8 by the solid curve. This curve was obtained from the numerical analysis of the measured spectrum of the output coupler, intracavity loss and gain profiles. As we can see from this figure, the behavior of the net-gain maximum corresponds to the Stokes frequency shift with the pulse energy growth, due to the gain coefficient decrease. However, the magnitude of this shift (~ 10 nm) is not sufficient to explain the experimental values (up to 50 nm). Besides that, the location of the pulse spectrum in general does not coincide with the net-gain maximum.

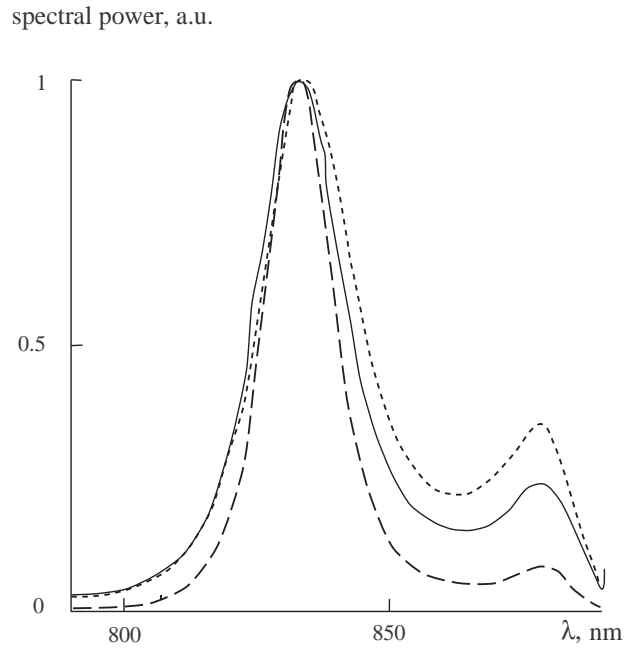


Figure 7. The dependence of generation spectra on wavelength in the presence of high-order dispersion in the distributed (solid and dash curves) and the discrete-element (dot) models. $\sigma = 1$, $\gamma = 0.05$. For the corresponding pulse parameters see Table 2.

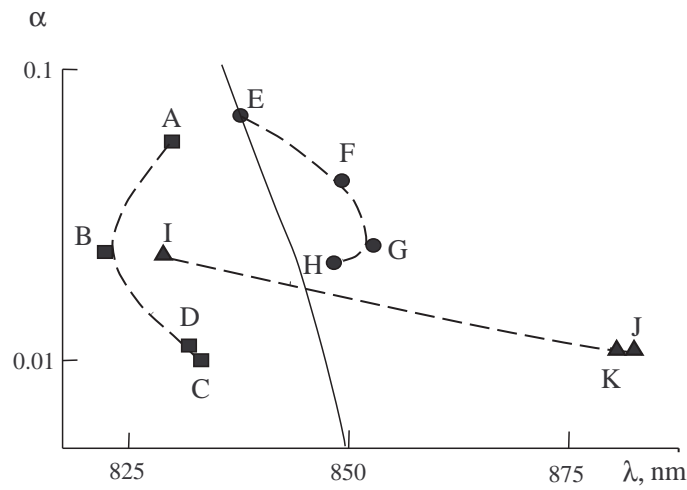


Figure 8. Pulse central wavelength as a function of the saturated gain coefficient. Solid line: Net-gain maximum; *ABCD* spectrum peak in the case of gain saturation without reabsorption and Raman scattering in the active medium; *EFGH* contribution of the reabsorption; *IJK* contribution of Raman scattering. Points correspond to Table 3.

Table 2. Normalized pump power, pulse duration and energy for Fig. 7

Line in Fig. 7	$P \times 10^4$	t_p , fs	E , nJ
solid	3.2	27	20
dash	2	30	12
dot	3	25	16

Table 3. Ultrashort pulse energies and durations for Fig. 8

Points	<i>A</i>	<i>B</i>	<i>C</i>	<i>D</i>	<i>E</i>	<i>F</i>	<i>G</i>	<i>H</i>	<i>I</i>	<i>J</i>	<i>K</i>
Energy, nJ	16	27	47	54	20	38	52	119	33	78	103
Pulse width, fs	45	28	20	23	28	20	18	37	25	14	19

To check the last thesis we performed numerical simulations on the basis of the described above model in the presence of dissipative factors only. The results are presented in Fig. 8 by the dashed lines *ABCD* and *EFGH*. The letters alongside of squares, circles and triangles denote the intracavity pulse energy obtained from the numerical simulation (see Table 3). The pulse energy variation results from the change of modulation parameter σ , i.e. due to the change of the cavity configuration.

The curve *ABCD* illustrates the case when there is no reabsorption and Raman scattering in the active medium. The dependence of frequency shift on pulse energy is not monotonous: at the minimum pulse width (15 fs in our case) there is no Stokes frequency shift, contradicting the experimental data. Moreover, the maximal shift (of about 6 nm) is by an order of magnitude less than that observed in the experiment. It is clear, that gain band asymmetry and output loss alone cannot produce large self-frequency shift in Cr:LiSGaF laser.

Stronger contribution is provided by the reabsorption in the active medium (curve *EFGH* on Fig. 8). For small energies the simulation result (point *E* on Fig. 8) coincides with the prediction made on the basis of elementary model of net-gain maximum shift (solid curve). The rise of the pulse energy increases the shift (up to 25 nm in our case), much more than in the previous case, although still by a factor of two less than in the experiment.

Note, that after certain pulse energy the spectral shift is again decreasing. This is caused by the increase of the pulse duration for the large energies (point *H* on Fig. 8), due to the nonlinear loss saturation, resulting in reduced spectrum width. The laser approaches the condition of the cw operation, described by solid curve (although the conditions of pulsed gain saturation strongly differ from those in cw-regime).

4.3. Raman scattering

As pointed out in the previous section, the net-gain shift model fails to provide correct description of the experimental data by a factor of two. However, taking the stimulated Raman scattering into account allows to obtain large frequency shifts, increasing with pulse energy growth. In Fig. 8 the curve *IJK* demonstrates the Raman scattering action in the absence of reabsorption effect. As the simulation demonstrates, the red components originate from the amplified Raman signal, which pulls the whole spectrum over the long wavelength limit at the given pump power, defined by the spectral filtering.

Note the pronounced threshold-like character of the effect. For the small energies (point *I*) the spectral shift is negligible, but the energy growth causes very strong shift (60 nm in our case) in good agreement with experimental results^{1,3,4} and with analytical prediction⁸. Since the gain saturation does not play important role in this case, the dependence of frequency shift on gain coefficient is insignificant.

As already mentioned above, the main contribution to the stimulated Raman process comes from the energy transfer from the blue part of the pulse spectrum (pump) to the red one (Stokes). The efficiency of the stimulated Raman scattering is therefore defined by the product of intensities at pump and Stokes frequencies. The separation between Stokes and pump components is fixed, it is equal to the Raman line frequency Ω_j . Therefore, decreasing the pulse spectrum width strongly suppresses the effect and reduces self-frequency shift. Assuming that the pulse spectrum has exponential fall-off to the blue and red sides, we see that the dependence of the Raman shift on the

pulse spectrum width should be asymptotically exponential at long pulse durations. This is also the result of the analytical theory in Ref.⁸ where sech^2 pulse shape has been assumed.

As the Raman effect strongly depends on the pulse intensity and Raman gain, it should be especially pronounced in low-gain lasers working with low output coupling and high intracavity pulse energy, such as Cr:LiSGaF, Cr:LiSAF, Cr:YAG. These materials also possess strong and broad Raman lines.⁹ Large power-dependent red-shift in Cr:LiSGaF and Cr:LiSAF is well documented.^{1,2,3} In femtosecond Cr:YAG lasers, femtosecond pulse spectrum is also always red-shifted with respect to the cw wavelength in the same resonator.¹⁴

4.4. Discrete-element model

Finally, we can compare the simulation results in case of distributed and discrete-element models. In the case of the high-order dispersion action the transition to the distributed-element model does not significantly change the spectral characteristics of the pulse (the dot curve in Fig. 6, *b*). The long-wavelength “shoulder” of the spectrum in the case of the net dispersion corresponding to solid curve in Fig. 6 *a* is somewhat stronger than in the distributed model. This is because this “shoulder” results from local dispersion maximum due to the chirped mirror (CM₁ on Fig. 1), which is the closest to the output mirror. Additionally, the self-phase modulation contribution is found to be slightly higher in comparison to the distributed model. However, all these changes are not qualitative. We found also that the transformation of the spectrum on each laser elements is small ensuring the validity of the distributed model. It should also be noted, that the transition from the distributed to the discrete model slightly increases the contribution of the Raman scattering, seen by the lower threshold energy.

5. CONCLUSION

Using the numerical simulations performed in the framework of one-dimensional distributed and discrete-element models, we analysed the spectral characteristics of a cw Kerr-lens mode-locked Cr: LiSGaF-laser. The two main factors causing the ultrashort pulse self-frequency shift have been established: the nonlinear shift of the net-gain band due to the gain saturation in the presence of reabsorption in the active medium and the stimulated Raman scattering. The first effect is essential for comparatively small pulse energies and produces wavelength shifts up to 30 nm. The Raman scattering occurs as a result of pulse energy growth and causes the large (over 50 nm) red shift. The contribution of the high-order dispersion (up to the eighth order), gain-band asymmetry and spectral characteristics of output coupler were estimated as well. However, their effect on the pulse central frequency is much smaller than that of the stimulated Raman scattering, which is the main cause of spectral red-shift in Kerr-lens modelocked laser. The shift values obtained from the numerical simulations are in good agreement with experimental data.

Analytical part of the calculations is presented on <http://www.geocities.com/optomapple>

ACKNOWLEDGMENTS

This work was supported by Austrian National Science Fund Projects T-64, P14704-PHY and Austrian National Bank Project 7913. V.L. Kalashnikov gratefully acknowledges support from the Austrian Science Fund (FWF), Project M611.

REFERENCES

1. I.T. Sorokina, E. Sorokin, and E. Wintner, A. Cassanho, H.P. Jenssen, R. Szipöcs. “14-fs pulse generation in Kerr-lens mode-locked prismless Cr:LiSGaF and Cr:LiSAF lasers: observation of pulse self-frequency shift,” *Opt. Lett.* **22**, pp. 1716–1718, 1997.
2. S. Uemura, K. Torizuka. “Generation of 12-fs pulses from a diode-pumped Kerr-lens mode-locked Cr:LiSAF laser,” *Opt. Lett.* **24**, pp. 780–782, 1997.
3. I.T. Sorokina, E. Sorokina, E. Wintner, A. Cassanho, H.P. Jenssen, R. Szipöcs. “Sub-20 fs pulse generation from the mirror dispersion controlled Cr:LiSGaF and Cr:LiSAF lasers,” *Appl. Phys. B* **65**, pp. 245–253, 1997.
4. I.T. Sorokina, E. Sorokin, and E. Wintner. “Femtosecond Cr:LiSGaF and Cr:LiSAF lasers: phenomena and limitations in the 15-fs regime,” in *ICONO’98: Ultrafast Phenomena and Interaction of Superstrong Laser Fields with Matter*, *Proc. SPIE* **3735**, pp. 2–21, 1999.
5. Ch. Spielmann, P. F. Curley, T. Brabec, F. Krausz, “Ultrabroadband Femtosecond Lasers,” *IEEE J. Quantum Electron.* **30**, pp. 1100–1114, 1994.

6. S.A.Akhmanov, V.A.Vysloukh, and A.S.Chirkin, *Optics of femtosecond laser pulses*, Chap. 1, Springer, New York., 1992.
7. J. Jasapara, V.L. Kalashnikov, D.O. Krimer, I.G. Poloyko, M. Lenzner, W. Rudolph, “Automodulation in Kerr-lens modelocked solid-state laser,” *J. Opt. Soc. Am.* **B 17**, pp. 319–326, 2000.
8. H.A. Haus, I. Sorokina, and E. Sorokin, “Raman-induced redshift of ultrashort mode-locked laser pulses,” *J. Opt. Soc. Am.* **B 15**, pp. 223–233, 1998.
9. I.T. Sorokina, E. Sorokin, E. Wintner, A. Cassanho, H.P. Jenssen, “Raman induced pulse self-frequency shift in the sub-20 fs Kerr-lens mode-locked Cr:LiSGaF and Cr:LiSAF lasers,” in *OSA Trends in Optics and Photonics series*, W. Bosenberg and M.M. Fejer, eds., **19**, p. 359, OSA, Washington DC, 1998.
10. K. M. Gäbel, R. Lebert, R. Poprawe, A. Valster, “Signature of the Raman self-frequency shift on the autocorrelation of sub-20-fs pulses from Colquiriite lasers,” in *Conf. on Lasers and Elecrto-Optics*, paper CThM48, OSA Techn. Digest series, pp. 483–484, 2000.
11. H. A. Haus, J. G. Fujimoto, E. P. Ippen, “Analytic theory of additive pulse and Kerr lens mode locking,” *IEEE J. Quant. Electr.* **QE-28**, pp. 2086–2097, 1992.
12. J. Herrmann, B. Wilhelmi, *Laser fur Ultrakurze Lichtimpulse*, Akademie-Verlag, Berlin (1984).
13. R.L. Sutherland. *Handbook of Nonlinear Optics*, p. 305, Marcel Decker, New York, 1996.
14. see e.g. A. Sennaroglu, C.R. Pollock, and H. Nathel, *Opt. Lett.* **19**, pp. 390–392, 1994; Y. Ishida and K. Naganuma, *Opt. Lett.* **19**, pp. 2003–2005, 1994; Zh. Zhang et al, *Opt. Lett.* **24**, pp. 1768-1770, 1999.